Journal of Water Process Engineering 32 (2019) 100924

Contents lists available at ScienceDirect

Journal of Water Process Engineering

journal homepage: www.elsevier.com/locate/jwpe

Optimization of the heterogeneous electro-Fenton process assisted by scrap zero-valent iron for treating textile wastewater: Assessment of toxicity and biodegradability

Edison GilPavas*, Santiago Correa-Sánchez

GIPAB: Grupo de Investigación en Procesos Ambientales, Departamento de Ingeniería de Procesos, Universidad EAFIT, Cr 49 # 7 Sur 50, Medellín, Colombia

ARTICLE INFO

Keywords:
Textile industrial wastewater
Electro-Fenton
Scrap zero-valent iron
Optimization
Toxicity

ABSTRACT

In this work, the heterogeneous electro-Fenton process assisted by scrap zero-valent iron (SZVI) and with graphite electrodes (as anode and cathode) is studied as an alternative way to treat wastewater from a textile plant located in Medellín, Colombia. The effects of the initial pH, SZVI load, and current density in the SZVI-assisted electro-oxidation process (EO/SZVI) are analyzed and optimized using multivariable regression models generated using the Box–Behnken experimental design and convex nonlinear optimization. The EO/SZVI process leads to maximum reductions of approximately 100%, 67%, and 59% in color, chemical oxygen demand (COD), total organic carbon (TOC), respectively, under the optimal operating conditions of pH of 3.5. Further, it leads to an SZVI concentration of 0.6 g/L, and a current density of 20 mA/cm^2 during 30 min of electrolysis. The post-process pollutants are characterized further using molecular weight distribution measurements, ultraviolet–visible spectroscopy, high-performance liquid chromatography, biodegradability, and toxicity. The results show that the treated effluent is polluted mostly by carboxylic acids of low molecular weight. A remarkable enhancement of the biodegradability of the effluent is evidenced by an increase in the BOD_5/COD ratio (biodegradability index) from 0.15 to 0.54. Although the EO/SZVI process does not improve the toxicity (as measured by the mortality of *Artemia salina*), the latter is reduced subsequently from 100% to 20% through adsorption using activated carbon (AC). The findings of this study indicate that the EO/SZVI process is an effective and promising alternative for treating textile wastewater.

1. Introduction

Industrial wastewater discharge is a matter of concern because of its high pollutant content [1,2]. Textile industrial wastewater (TIWW) generated owing to the typical textile manufacturing process, which is diverse and contains various dyes and other chemicals (e.g., fabric softeners, salts, pesticides, coupling agents, polishing and coating agents, and surfactants). Therefore, conventional treatment is therefore not viable, and only a few other types of treatment are effective; more complex reactions are required to degrade the compounds in such matrices [3]. The textile industry uses organic additives such as dyes and surfactants. It is among the most prolific producers of wastewater, which has poor biodegradability and high toxicity and/or mutagenicity. Because of its high content of persistent organic pollutants, TIWW cannot be treated by conventional means [2,4]. Therefore, TIWW treatment has received considerable research attention.

Several TIWW treatment methods have been reported in the literature [5–9], including electrochemical advanced oxidation processes (EAOPs). The efficacy of EAOPs has been demonstrated for the organic pollutants in TIWW; moreover, EAOPs are highly environmentally compatible, which distinguishes them from other processes [1,10]. Among EAOPs, those based on Fenton chemistry have been studied as viable treatment alternatives, achieving satisfactory degradation in TIWW [11,12]. However, EAOPs exhibit drawbacks such as the following: (i) high electrical energy requirements and (ii) the need for expensive materials, such as boron-doped diamond; these challenges have been addressed in recent studies [1,10,13].

The electro-Fenton (EF) process is a widely known Fenton-based EAOP. As described in Eqs. (1) and (2), the EF process uses hydroxyl radicals ($^{\bullet}OH$) produced by the reaction of electrogenerated hydrogen peroxide (H_2O_2) and ferrous ions (Fe^{2+}) that are either added to the solution or released by an iron source [1,13]:

$$Cathode:\ O_2 + 2H^+ + 2e^- \rightarrow H_2O_2 \quad (1)$$

* Corresponding author.
E-mail address: egil@eafit.edu.co (E. GilPavas).

https://doi.org/10.1016/j.jwpe.2019.100924
Received 4 March 2019; Received in revised form 13 August 2019; Accepted 18 August 2019
Available online 26 August 2019

$$Fe^{2+} + H_2O_2 + H^+ \rightarrow Fe^{3+} + HO^{\bullet} + H_2O \quad (2)$$

Although the EF process is highly efficient for degrading several persistent organic pollutants, including those in TIWW [14,15], this process has the following major setbacks: (i) the EF process is only optimal under strong acidic conditions, requiring a post-process step to neutralize the pH of the effluent before discharge. (ii) Because the catalyst (Fe^{2+}) is dissolved, it is non-recyclable. (iii) The EF process has a high energy consumption [11,16,17]. (iv) The electro-oxidation (EO) process may generate organochlorine compounds in the presence of chlorine, as well as other intermediaries that are more toxic than the parent compounds [18].

To address the non-recyclability of iron, previous studies have explored the use of heterogeneous iron-containing catalytic sources for decomposing H_2O_2. This approach can optimize the catalytic consumption and widen the pH range of this process, which can reduce the cost of controlling the pH before and after the process. Different methods have been studied for applying heterogeneous EF methods, including the use of natural iron-bearing materials [19,20], synthetic catalysts containing iron [7,13], and cathodic materials containing iron oxides and other transition metals, which act as both the cathode and iron source [1,4,13]. However, the use of these iron-bearing catalysts makes the process more expensive; therefore, further research is required.

In a previous work, scrap zero-valent iron (SZVI) was successfully applied as a heterogeneous source of iron to produce reactive oxygen species through Fenton-like chemistry, as shown in Eqs. (3) and (4) [21]:

$$Fe^0 + H_2O_2 + 2H^+ \rightarrow Fe^{2+} + 2H_2O \quad (3)$$

$$Fe^{2+} + H_2O_2 \rightarrow HO^{\bullet} + OH^- + Fe^{3+} \quad (4)$$

Several studies have reported the use of SZVI in various pollutants and wastewater effluents [10,22–24]. This approach is a promising alternative because it reuses residues from another industry and is inexpensive.

Previous studies have reported a high concentration of chloride (Cl^-) in TIWW, at 1600–2100 mg/L owing to the high amount of NaCl in TIWW. Therefore, carcinogenic and toxic chlorinated organic compounds may be generated during the electrochemical reaction [18]. Consequently, the toxicity of the post-process sample must be considered prior to discharge. If necessary, additional steps that have been used to successfully resolve toxicity issues, such as adsorption using activated carbon (AC), must be included in the process [25].

Although ZVI-assisted Fenton-like systems have been effective for water treatment in the past, to the best of our knowledge, no previous studies have used ZVI in a heterogeneous EF system. Moreover, most studies have only examined color removal in synthetic effluents containing indigo or indigo carmine dye [26,27], with few studies published on the use of real indigo dyeing effluents [28,29]. The characterization and experimentation of such effluents are necessary because unlike synthetic effluents, real effluents exhibit unpredictable behavior; for example, processes that have been examined in synthetic dyed water may lead to different results under practical conditions. Moreover, few studies have used SZVI as a catalyst to treat actual industrial wastewater [21,23,30]; to the best of our knowledge, the decontamination of real indigo dyeing effluent by an EO/SZVI/AC process has not yet been studied.

Therefore, this work focuses on the development of an effective treatment for real wastewater produced by the indigo dyeing and textile finishing processes of a local jeans factory, which is not amenable to biodegradation. This treatment was achieved by an EO/SZVI process, in which the pH, SZVI load, and current density (*j*) were optimized to minimize the operational cost while maintaining a sufficient chemical oxygen demand (COD) reduction and color degradation. The optimization was performed by using a Box–Behnken experimental design (BBD) coupled with nonlinear optimization under certain restrictions. Changes in environmentally relevant parameters, such as biodegradability and toxicity, were monitored; subsequently, the total operating cost (OC) was optimized.

2. Materials and Methods

2.1. Sample handling and characterization

A sample of TIWW was collected from a homogenization tank at the end of the process of a textile manufacturing plant located in Medellín, Colombia. The sample was stored at 4 °C to prevent self-degradation, and periodic measures of COD, TOC, and absorbance (660 nm) were performed as indicators that the sample did not change over time.

An initial characterization of the sample was performed to serve as the baseline against which to compare the parameters of the post-treatment sample. Different parameters were measured in duplicate using an ultraviolet–visible (UV–vis) double-beam spectrophotometer (Spectronic Genesys 2PC) and following the standard methods of the American Public Health Association [31]. The UV–vis spectrum was measured in the range of 200–700 nm to monitor the behavior of organic aromatic pollutants. Moreover, absorbance at 660 nm and true coloration (TC) (ISO 7887: 2011) served as indicators of the blue coloration in the sample. The COD (method 5220D) and TOC (method 5310D) were measured as indicators of the content of organic pollutants in the sample. Biodegradability was assessed by the proportion of BOD_5 (method 5210B) in relation to COD, and the toxicity was assessed by checking the mortality of *Artemia salina* when exposed to the sample by following the method used by Manfra et al. [32]. Further, the turbidity (method 2130B) and total solids (2540B) were measured as indicators of the quality of the sample. The Cl^- content was determined using the standard Volhard titrimetric argentometry method and found to be 1856.8 mg/L. The surface structure of the SZVI was studied using a scanning electron microscope (SEM, JEOL JSM-5910 LV, Ltd., Tokyo, Japan) coupled to an X-ray analyzer with energy dispersion to assess the morphology and elemental composition before and after treatment. The point of zero charge of the SZVI was determined by the solid addition method [33]. Seven samples were prepared by adjusting the pH of 45-mL 0.1-mol/L NaCl solution to 3, 4, 5, 6, 7, 8, and 9 by adding either 0.1-M HCl or 0.1-M NaOH. Then, the solution volume was adjusted to exactly 50 mL with 0.1-mol/L NaCl solution. Next, 0.1-g SZVI was added, and the samples were stirred for 48 h. Subsequently, the final pH (pH_f) of each sample was measured, and the difference between the initial pH (pH_i) and pH_f of each sample was plotted against pH_i. The pH value at the x-intercept in the resultant graph was considered as the point of zero charge (pH_{PZC}).

2.2. SZVI/EO process

Experiments were performed in an 80-mL glass cylindrical reactor containing TIWW at a temperature of 25 °C and with an agitation speed of 400 rpm that kept the SZVI suspended in the aqueous phase. Graphite electrodes (1.5 × 3.3 × 0.6 cm^3) were used as the anode and cathode with a fixed submerged area, and the electric current was set to achieve the desired current density. The pH of the aqueous phase was adjusted with H_2SO_4 (Merck; 98% purity), and the gap between the electrodes was fixed to 1 cm. To remove impurities, the SZVI (80% purity) was first washed in NaOH (4.5 M) for 30 min and subsequently in HCl (5 M) for 30 min. Then, it was washed three times with deionized water to remove the residual Fe^{2+} and HCl.

Parameters such as the pH, current density *j* [mA/cm^2], and SZVI load were determined using a Box–Behnken experimental design (BBD) to obtain regression models for the percentage of color removal, percentage of COD removal, and OC, which were used to analyze the parameters and optimize them by means of the response-surface methodology and nonlinear convex optimization. Experimental runs of 30 min were performed, and the COD and TOC of the post-process

sample were measured to determine the percentages of COD degradation (%DCOD) and color degradation (%DC), which served as response variables for the experimental design. Any residual H_2O_2 was quenched with MnO_2 (Sigma Aldrich; reagent grade ≥ 90%) before the COD measurements to prevent measurement interference due to its presence.

The results of the BBD were analyzed using the Statgraphics Centurion XVI software and fitted to a quadratic model to generate a three-dimensional response-surface plot to visualize the individual and interaction effects of the factors. Additionally, the OC of the process was calculated as shown in Eq. (5) [4]:

$$OC\left(\frac{USD}{m^3}\right) = \frac{\alpha * I * \bar{V} * t}{v} + \sum \beta_i RC_i \quad (5)$$

where α is the cost of electricity (USD/kWh), I is the current during the process, $\bar{V}$ is the average voltage during the process, t is the process time, v is the volume of the batch, β_i is the cost of reactant i (USD/kg), and RC_i is the quantity of reactant i.

2.3. Optimization of parameters

The experimental results were fitted to the regression model that correlates them with the process parameters by an empirical second-order model of the form:

$$Y_i = \beta_0 + \sum_{i=1}^{3} \beta_i x_i + \sum_{i=1}^{3} \beta_i x_i^2 + \sum_{i=1}^{3} \sum_{j=1}^{3} \beta_{ij} x_i x_j \quad (6)$$

where β_0, β_i, and β_{ij} are the regression coefficients for the different variables and x_i and x_j are the independent variables. The model was achieved via multivariable regression using R-project software [34], and analysis of variance (ANOVA) was applied to study the fitting of the model based on the F-test, R^2, and adj R^2. This model can be used to predict the different response variables according to the operational variables. Additionally, it was used to generate response-surface plots that show the effects of the different variables and their interactions. However, this approach is only useful for optimizing individual variables, i.e., to find the parameter values that maximize or minimize one of the response variables. Because it is necessary to find the lowest cost in the acceptable region of %DCOD and %DC, the process was optimized through nonlinear convex optimization with the following restrictions:

$$min\ OC = \beta_{0OC} + \sum_{i=1}^{3} \beta_{iOC} x_i + \sum_{i=1}^{3} \beta_{iOC} x_i^2 + \sum_{i=1}^{3} \sum_{j=1}^{3} \beta_{ijOC} x_i x_j, \quad (7)$$

$$DCOD = \beta_{0COD} + \sum_{i=1}^{3} \beta_{iCOD} x_i + \sum_{i=1}^{3} \beta_{iCOD} x_i^2 + \sum_{i=1}^{3} \sum_{j=1}^{3} \beta_{ijCOD} x_i x_j \quad (8)$$

$$DCOD \geq MinDCOD \quad (9)$$

where OC and $DCOD$ are the OC and COD degradation, respectively, β_o, β_i, and β_{ij} are the regression coefficients for the OC and COD, and $MinDCOD$ is the minimum acceptable COD degradation. Notice that, although the regression coefficients may be different for OC and $DCOD$, x_i and x_j are the same in both equations; further, their values are restricted to the studied range. Nonlinear programming in Microsoft Excel was used to calculate the conditions that minimize OC while keeping $DCOD$ higher than the minimum value required to comply with regulations ($DCOD_{min}$).

2.4. Characterization of post-process effluent

Then, experimental runs under the calculated optimal conditions were performed to further characterize the post-process compounds and compare the performances of the SZVI/EO and EF processes. The output of the reaction was monitored for 1 h for %DCOD, %DTOC, TOC degradation, BOD_5/DQO ratio, molecular weight distribution (MWD), concentration of carboxylic acid intermediates [through high-performance liquid chromatography (HPLC)], and toxicity. These runs served the following objectives: (i) better understand how the reaction behaves over time, (ii) assess the ability of the quadratic model to predict %DC and %DCOD accurately, and (iii) analyze the effectiveness of the process at improving the environmentally relevant parameters.

2.4.1. Handling of A.Salina and toxicity assessment

Acute toxicity tests with *A. salina* (Carolina Biological Supply Company) were performed in duplicate before and after the process, following the method used by da Costa Filho et al. [35]. The *A. salina* were bred beforehand for 24 h in an aqueous growth medium resembling the conditions needed for these microcrustaceans to survive and develop (35 g/L NaCl; lateral illumination of 3500 lx; 25 °C). Then, test plates containing 20 *A. salina* crustaceans in 9.5 mL of the sample solution and 0.5 mL of saline medium were incubated for 24 h, and no nourishment was provided to these crustaceans between hatching and testing. Immobilization was observed after 24 h of incubation. The crustaceans were considered immobile if they remained still for 15 s of observation. Acute toxicity is expressed as the percentage of immobilization compared with a nontoxic control. The mortality of *A. salina* was calculated as follows:

$$Mortality\ (\%) = \left(\frac{N_0 - N_t}{N_0}\right) x100, \quad (10)$$

where N_0 is the initial number of crustaceans and N_t is the number of crustaceans alive after exposure to the post-treatment sample for a period of time t.

2.4.2. MWD and characterization of intermediate carboxylic acids

Ultrafiltration (UF) was used to separate the sample into five fractions according to their MWD. Ultracell regenerated cellulose membranes of 44.5 mm (Millipore Corporation) with molecular weight (MW) cut-offs of 3, 5, 10, and 30 kDa were used to separate the pollutants according to their MWD. The membranes were stored in an aqueous solution of 10% ethanol at 4 °C, and they were washed with 0.1-M NaOH for 30 min and flushed with deionized water before usage, following the manufacturer's instructions. The UF was performed in a 50-mL Amicon stirred-cell UF system (Millipore–Merck), and the operational UF pressure was kept constant at 0.4 MPa using a steady supply of highly pure N_2 (99.999%). The sample was filtrated through the membranes, and the first 5 mL of filtrate was discarded to prevent cross contamination due to membrane fouling. Then, the TOC was measured for each filtrate as an indicator of the organic-matter concentration of each fraction.

Furthermore, ion-exclusion chromatograms were performed in the sample to better understand the generation and degradation of carboxylic acids as intermediaries in the process. This was done using an Agilent 1200 liquid chromatograph equipped with a Hi-Plex H, column (300 mm and 7.8 mm (i.d.)), at 35 °C and coupled with a photodiode array detector at λ = 210 nm. 20-μL aliquots were injected into the liquid chromatograph under circulation of 4-mM H_2SO_4 at 0.6 mL/min as the mobile phase [36]. Benzoquinone (BQ) and tert-butyl alcohol (t-BuOH) were used as scavengers to analyze the proposed reaction mechanism, these were reagent grade used without further purification and purchased from Merck.

3. Results and discussion

3.1. Physicochemical analysis of SZVI

The surface morphology and structure of SZVI before and after EO/SZVI treatment were studied by SEM-EDX analysis. The SEM-EDX results for new and used SZVI are shown in Fig. S1. The particles exhibit irregular shapes in the range of 83–600 μm. As shown in Fig. S1 (Supplementary Information), the texture of the used SZVI differs from that of the initial surface (with substantial deposition on the surface) due to the oxidation–reduction of SZVI [see Eq. (2)], coagulation of iron hydroxides, adsorption of molecules, and/or adherence of the reaction by-products. Further, these features are reflected in the differences in the elemental composition results obtained by SEM-EDX. The decrease in the Fe percentage in the SZVI from 80.2 to 71.77 can be attributed to the generation of Fe^{2+} ions, which are produced by the oxidation of SZVI and subsequently released to the solution. The increased O_2 level in the composition confirms the increase in Fe oxides adhering to the SZVI surface.

The point of zero charge for SZVI was determined using the solid addition method described by Mortazavian et al. [33], resulting in $pHzpc_{,SZVI} = 7.2$ (see Fig. S2, Supplemental Information). This result indicates that the SZVI surface is positively and negatively charged at pH values lower and higher than 7.2 by attracting and repelling anions, respectively. Additionally, Li et al. [37] found a similar pH_{zpc} value of 7.4 for nZVI in the remediation of Cr (VI)-polluted water.

3.2. Sample characterization

The characteristics of the studied sample are summarized in Table 1 with the Colombian emission limits and treatment efficiency (under optimal conditions). Notice that the COD of the raw sample does not comply with regulations, whereas that of the post-process sample does. Furthermore, notice that the biodegradability index (DBO_5/DQO) increased from 0.15 to 0.54, which suggests that the process increased the sample's biodegradability to a level that is acceptable for discharge.

3.3. BBD experimental results: model fit and statistical analysis

A BBD was performed with pH, SZVI load, and current density as factors and %DC, %DCOD, and OC as response variables; Table 2 shows the experimental runs and results of the BBD.

Experimental data for each response variable were fitted to a quadratic model for multivariate regression analysis using R-project software (https://www.r-project.org/). The ANOVA results for the regression models are presented in Table 3. The R^2 and R^2_{Adj} values of 0.96 and 0.92 for %DCOD, 0.97 and 0.92 for %DC, and 0.96 and 0.91 for OC show that the variability in the data can be effectively explained by the model. Moreover, an F-test was performed to verify the significance of the models; p-values lower than the significance level ($\alpha = 0.05$) indicate that the model provides a better fit than the intercept-only model (i.e., the model is significant). As shown in Table 3, the p-values of the models for %DCOD, %DC, and OC are 0.003, 0.002, and 0.002, respectively, indicating that all the models are significant. Table 3 shows the p-values for the independent variables and interactions; p-values below $\alpha = 0.05$ indicate that the model with the respective variable provides a better fit than the model without that variable (i.e., the variable is significant). The results show that pH, *j*, and the SZVI:*j* interaction are significant for %DCOD, pH, SZVI, *j*, and SZVI:*j* are significant for %DC, and only *j* is significant for OC. Several nested models were proposed and compared through the Akaike information criterion (AIC) (not shown here). Those that yielded the best fit are presented in Eqs. (11–13).

Table 2
Experimental results of the EO/SZVI process for %DCOD, %DC, and OC according to the BBD. Electrolysis time: 30 min.

Run	pH	SZVI (g/L)	*j* (mA/cm^2)	%DC		%DCOD		OC (USD/m^3)	pH_{final}	*Va
				Y_{exp}	Y_{pred}	Y_{exp}	Y_{pred}			
1	4.5	5	20	87.39	84.63	40	41.13	4.11	5.5	11.8
2	3	2.8	10	91.82	88.13	48	46.88	1.91	3.6	9.4
3	4.5	2.8	15	80.0	81.33	43	43.67	3.05	5.1	11.5
4	3	0.6	15	95.91	97.5	62	64.25	3.17	3.3	11.3
5	6	2.8	20	78.45	81.88	38	39.13	4.28	5.1	12.3
6	4.5	0.6	20	94.55	92.38	61	57.38	4.11	5.4	11.8
7	3	2.8	20	98.27	99.13	67	68.38	3.52	4.6	9.5
8	4.5	5	10	82.72	85.63	44	47.63	1.72	5.3	9.3
9	6	2.8	10	60.36	58.88	34	32.63	1.48	5.7	7.9
10	4.5	0.6	10	55.18	57.38	24	22.88	1.34	5.2	7.1
11	6	5	15	86.0	84.5	49	46.75	2.69	5.8	10.1
12	4.5	2.8	15	82.63	81.33	46	43.67	3.05	5.2	10.1
13	4.5	2.8	15	81.0	81.33	42	43.67	3.05	5.1	11.8
14	3	5	15	94.89	97.25	61	58.5	2.80	5.3	9.8
15	6	0.6	15	65.0	63.75	30	32.5	3.1	5.6	11.7

* Va: Average Voltage.

Table 1
Characterization of textile industrial wastewater (TIWW) before and after EO/SZVI and EO treatment, and efficiency under optimal operating conditions. Electrolysis time: 60 min.

Parameter	TIWW	Emission limit[a]	Treatment		Treatment efficiency (%)	
			EO/SZVI	EO	EO/SZVI	EO
pH	6.1	6–9	3.8	4	–	–
Conductivity (mS/cm)	5.6	–	3.71	3.46	–	–
Turbidity (NTU)	261	–	3	0	98.85	100
COD (mg O_2/L)	704	400	112	270	84.1	62
TOC (mg O_2/L)	194	–	56	92	71.1	53
BOD_5 (mg O_2/L)	105.6	200	58.05	95.5	45	10
Absorbance (660 nm)	1.474	–	0.003	0.432	99.8	71
True Color (mg Pt /L, C) ISO 7887:2012-04 (B,C)	1286	–	62	184	95.2	85.6
λ = 436m (m^{-1},B)	$\lambda_{436} = 85$	———	$\lambda_{436} = 4.1$	$\lambda_{436} = 6.5$	95 (λ_{436})	92 (λ_{436})
λ = 525m (m^{-1},B)	$\lambda_{525} = 78$		$\lambda_{525} = 1.8$	$\lambda_{525} = 4.1$	98 (λ_{525})	95 (λ_{525})
λ = 620 m (m^{-1},B)	$\lambda_{620} = 68$		$\lambda_{620} = 1.5$	$\lambda_{620} = 3.4$	98 (λ_{620})	95 (λ_{620})
BOD_5/COD	0.15	0.4	0.54	0.35	–	–
Toxicity (% mortality of *A. salina*)	100	–	100	100	–	–
Generated sludge (kg/m^3)	———	———	0.054	0	–	–
OC (USD/m^3)			6.78	6.78	–	–

[a] Emission limit values for industrial wastewater discharge into the municipal sewer system according to Res. 0631, 17/03/2015, issued by the Ministry of Environment and Sustainable Development of Colombia (South America).

Table 3
ANOVA results for %DC, %DCOD, and OC as a function of the initial pH, SZVI load, and current density (*j*). Electrolysis time: 30 min.

	%DCOD					%DC				OC				
Source	Df	Sum sq	Mean sq	F value	p-value	Df	Sum sq	Mean sq	F value	p-value	Df	Sum sq	Mean sq	F value	p-value
pH	1	0.092	0.092	70.297	0.000	1	0.108	0.108	77.315	0.000	1	0.002	0.002	0.031	0.868
SZVI	1	0.004	0.004	2.703	0.161	1	0.021	0.021	15.027	0.012	1	0.019	0.019	0.260	0.632
j	1	0.039	0.039	29.432	0.003	1	0.058	0.058	41.335	0.001	1	11.450	11.450	153.035	0.000
pH^2	1	0.011	0.011	8.526	0.033	1	0.004	0.004	2.914	0.149	1	0.000	0.000	0.004	0.950
$SZVI^2$	1	0.001	0.001	0.524	0.502	1	0.001	0.001	0.523	0.502	1	0.001	0.001	0.009	0.928
j^2	1	0.003	0.003	1.949	0.222	1	0.002	0.002	1.706	0.248	1	0.072	0.072	0.960	0.372
pH:SZVI	1	0.009	0.009	7.149	0.044	1	0.011	0.011	7.884	0.038	1	0.000	0.000	0.003	0.960
pH:*j*	1	0.005	0.005	3.905	0.105	1	0.004	0.004	2.574	0.170	1	0.352	0.352	4.703	0.082
SZVI:*j*	1	0.039	0.039	29.851	0.003	1	0.032	0.032	23.170	0.005	1	0.034	0.034	0.457	0.529
Residual	5	0.007	0.001	*NA*	*NA*	5	0.007	0.001	*NA*	*NA*	5	0.374	0.075	*NA*	*NA*
	R^2	**R^2_{Adj}**	**Residual st er**	**F statistic**	**p-value**	**R^2**	**R^2_{Adj}**	**Residual st er**	**F statistic**	**p-value**	**R^2**	**R^2_{Adj}**	**Residual st er**	**F statistic**	**p-value**
Model	0.96	0.91	0.036	17.15	0.003	0.97	0.92	0.0373	19.16	0.002	0.9696	0.9149	0.273	17.72	0.0028

$$\%DC = 10.48 - 31.04*pH + 6.05*SZVI + 5.24*j + 1.43*(pH)^2 + 1.59*pH*SZVI + 0.4*pH*j + 0.25*(SZVI)^2 - 0.82*SZVI*j - 0.1*(j)^2 \quad (11)$$

$$\%DCOD = 28.43 - 26.66*pH + 6.78*SZVI + 9.36*j + 2.52*(pH)^2 + 1.52*pH*SZVI - 0.5*pH*j + 0.24*(SZVI)^2 - 0.93*SZVI*j - 0.103*(j)^2 \quad (12)$$

$$OC\left(\frac{USD}{m^3}\right) = 0.732 - 0.581*pH + 0.227*j + 0.0395*pH*j - 0.0056*(j)^2 \quad (13)$$

A Breusch–Pagan test was performed to verify the homoscedasticity of residuals in these models; p-values of 0.12, 0.09, and 0.45 for DCOD, DC, and OC, respectively, indicate that the models are homoscedastic, fulfilling the linear regression assumption.

3.4. Variable effects and optimization

The regression models were used to determine the optimal conditions of the process through nonlinear programming, the objective being to minimize the OC while maintaining a %DCOD of at least 73%. The lowest cost was achieved with a pH of 3.5, SZVI concentration of 0.6 g/L, and $j = 20$ mA/cm^2. This is shown in Fig. 1, which shows the response surfaces for %DCOD and OC. Fig. 1(a,c and e) show how *j* and the pH contribute to %DC, %DCOD, and the OC. Clearly, %DC and %DCOD both increase with *j*, with the latter being a highly important variable in any electrochemical treatment and one that influences the process efficiency and OC significantly. The production rates of H_2O_2 Eq. (1) and $^{\bullet}$OH Eq. (2) are controlled mainly by *j* during electrolysis. As shown in Fig. 1(a–d), *j* had the greatest impact on %DC, %DCOD, and OC among the studied variables. It has been reported that the removal efficiencies increase with *j* in the range of 10–20 mA/cm^2 because of the higher production of oxidant species, such as $^{\bullet}$OH, H_2O_2, and active chlorine species. [36].

According to the plots shown in Fig. 1, the TIWW was degraded most rapidly by EO/SZVI under acidic conditions, particularly at a pH value of approximately 3. This is because a pH value of 3.0 allows the largest concentration of the active Fe^{2+} species and the lowest rate of H_2O_2 parasitic decomposition [18]. Furthermore, the pH of the solution has a significant impact on the oxidation potential of ferrous ions in EF—the concentrations of Fe^{2+} ions and $^{\bullet}$OH radicals are easily affected by changing the concentration of hydronium ions, which is pH-dependent [21]. At a pH value of approximately 6, divalent iron ions are easily precipitated as iron (II) hydroxide because the precipitation of divalent iron depends on the pH, as is well known.

Several SZVI concentrations from 0.6 to 5 g/L were tested, and the results are shown in Fig. 1(b) and (d). Clearly, in the studied range of iron concentration, a high oxidation yield was achieved. At $j = 10$ mA/cm^2, the oxidation rate increases with the SZVI concentration, but if *j* and the SZVI concentration are both increased, then the process yield worsens notably. This phenomenon can be attributed to the parasitic reactions resulting from over dosing SZVI as a ferrous ion source [38], observed a similar trend for the effects of *j* and the pH.

Fig. 1(e) and (f) show how *j*, pH, and SZVI concentration affect OC. Clearly, the electrochemical cell OC increases with *j*. Further, a technically efficient process must be economically feasible. The major EO/SZVI OC is the electrical energy consumed during treatment. Increasing *j* and the electrolysis time enhances the efficiency of EO/SZVI; however, it also raises the cell voltage, energy consumption, and OC. Therefore, it is important to consider achieving the desired degradation with the lowest cost possible.

It has been widely reported that H_2O_2 can be electrogenerated by the two-electron reduction of O_2 on the surface of graphite anodes with a high surface area during EO [18]. H_2O_2 is expected to react with iron

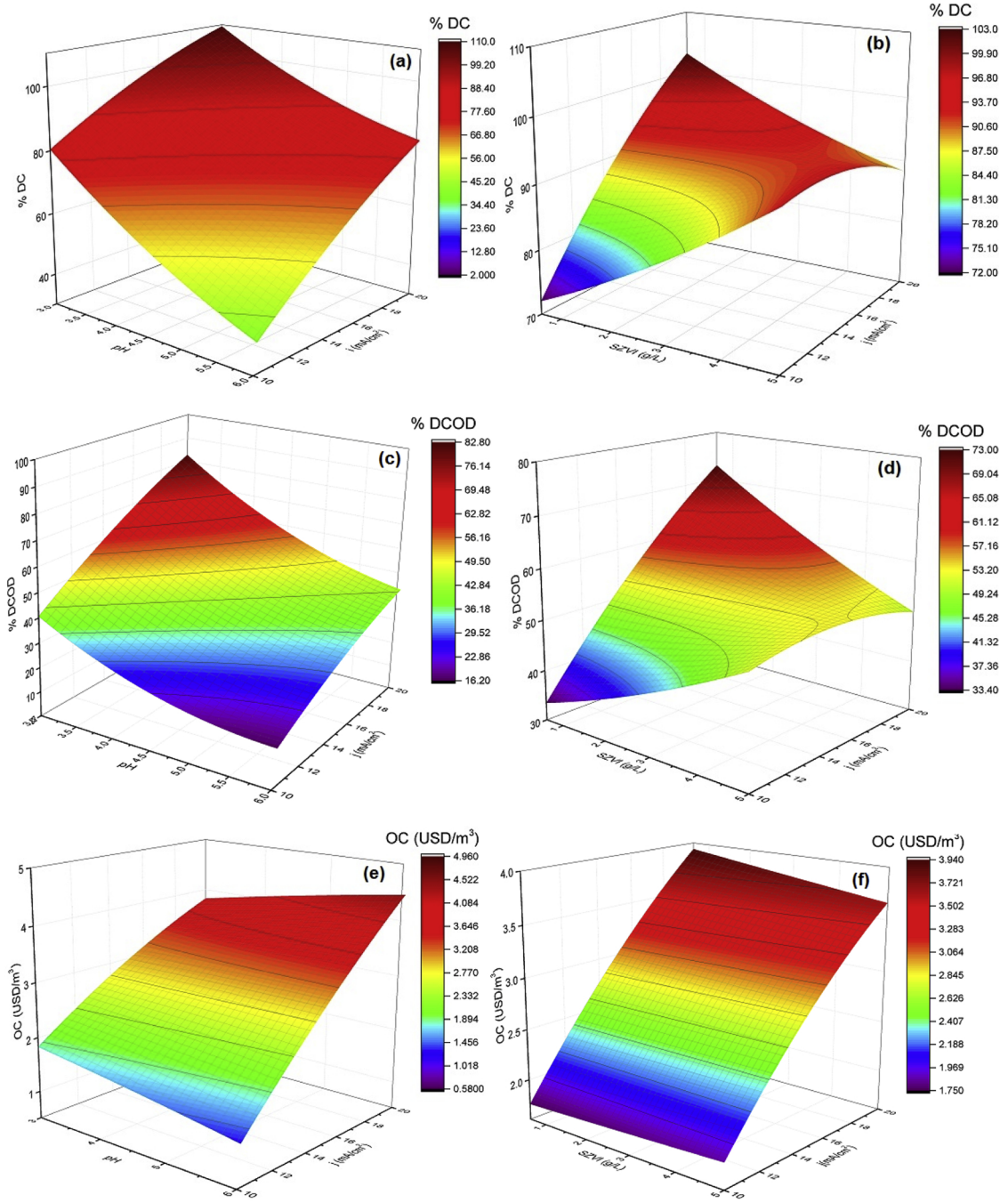

Fig. 1. Three-dimensional response surfaces generated from the BBD method using Eq. (10) for %DC (a, b), Eq. (11) for %DCOD (c, d), and Eq. (12) for OC (e). These are used to obtain the most important pair of factors. The reaction time was 30 min.

oxides on the surface of the SZVI to form $^{\bullet}OH$ in a Fenton-like process. Because little consumption of SZVI occurs during the process, the effect of the SZVI dosage is most likely associated with an increase in the surface area of the SZVI. The experimental results indicate that the effect of the SZVI load in the studied range is positive and significant for %DC but not for %DCOD or cost. This trend most likely arises because the reaction is primarily limited by the generation of H_2O_2 and only a fraction of the active iron sites are used during the reaction [13].

However, the interaction between SZVI and *j* is even more significant than that of SZVI. This can be explained from the various reactions that can occur during the EO process with a graphite anode: (i) the electro-generation of highly oxidant-active chlorine from the salt that remains from the textile dyeing process, (ii) the production of chemisorbed hydroxyl radicals from dissolved oxygen, and (iii) the aforementioned production of H_2O_2 from dissolved oxygen, which likely produces even more $^{\bullet}OH$ radicals in the Fenton-like reaction. All three reactions are mediated by the electrical current that is applied: a higher current density will accelerate the rate of production of the different oxidizing species, consequently increasing the rate of degradation. This agrees with the experimental results; as shown in Fig. 1(a) and (b), increasing the current density from 10 to 20 mA/cm^2 increases %DC by 20% and %DCOD by 25%. In agreement with this, notice that *j* is a significant factor for all variables. However, because *j* is the most cost-intensive parameter, it is necessary to minimize it to optimize the OC.

As mentioned before, a Fenton-like reaction occurs when the electrogenerated H_2O_2 reacts with the iron oxides on the surface of the SZVI. It has been widely reported that the Fenton process is more

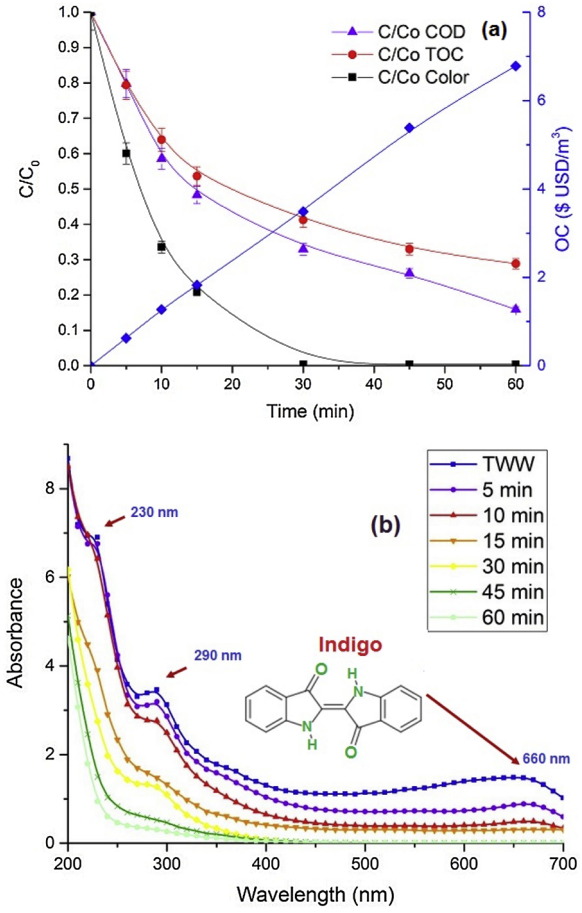

Fig. 2. Degradation of organic matter during 1 h of the EO/SZVI process under optimal conditions (pH = 3.5, SZVI = 0.6 g/L, and j = 20 mA/cm^2): (a) COD, TOC, color, and OC; (b) UV–vis spectrum. The error bars (smaller than the symbol if not visible) indicate the standard deviation.

efficient at pH of approximately 3 [18]. Therefore, it is expected that acidic conditions significantly increase $^{\bullet}$OH generation and the subsequent organic-matter degradation, matching the experimental results. Notice that in Fig. 1, where it can be seen that %DC and %DCOD are both higher under acidic conditions, a pH of approximately 3 yielded a %DCOD of approximately 83%, whereas a pH of 6 yielded only 43% with j = 20 mA/cm^2. Furthermore, it is important to remark that alkaline conditions favor other paths of degradation, such as coagulation (because of the production of hydroxides and polyhydroxides) and reductive pathways [39], which is why an increase in %DCOD can be seen from a pH of 6 onward. However, these pathways are much less efficient than the ones favored under acidic conditions: the yield at a pH of 9 was 33% less %DCOD than that at a pH of 3. Moreover, it has been reported that using SZVI can increase the effective working range for generating $^{\bullet}$OH radicals [40], which explains why a pH of 3.5 is acceptable for maintaining a high COD degradation while lowering OC. This cost is associated with the amount of reactant that is used to lower the pH of the effluent and then neutralize it after the process [21].

3.5. Kinetic study and mechanism analysis

The color removal, COD degradation (%DCOD), and TOC degradation (%DTOC) over time during the EO/SZVI process are summarized in Fig. 2(a). Notice that the color is removed almost completely after 30 min of reaction, and %DCOD and %DTOC show that organic-matter degradation occurs rapidly during the first 15 min and subsequently slows down. Because the increase in the process yields between 30 and 60 min are only 17% and 12% for %DCOD and %DTOC, respectively, while being almost 200% for the OC, it seems logical to select 30 min as the operating time for the process. Further, notice that as shown in Fig. 2(b), the initial TIWW sample showed three main absorption bands (λ) at (i) 220 nm, (ii) 270 nm (λ = 200–250 nm corresponds to the presence of primary-band acids, phthalates, ketones, aldehydes, alkanes, esters, etc., and λ = 250–275 nm corresponds to secondary-band alcohols, aldehydes, ketones, etc.) [41], and (iii) 660 nm, corresponding to the indigo dye. After 30 min of the process, the band at 660 nm had disappeared almost completely and the sample was almost colorless. After 60 min, the peak at λ ≈ 220 nm had disappeared completely. This shows that the organic matter was degraded/oxidized by the oxidant species ($^{\bullet}$OH, H_2O_2, HOCl, etc.), with only a low-intensity band remaining at λ ≈ 270 nm, indicating the presence of some organic remnants that are attributed to intermediate degradation compounds. It was found that the cell voltage decreased between 7.5% and 10% during the process time while keeping current density at a constant value, this is because the cell resistance decreases due to the changes in the matrix (see Fig. S3, Supplemental Information).

It should be noted that the EO/SZVI system was not simply a combination of EO and SZVI processes because a different reaction (Fenton reaction) was expected in this case. At the graphite cathode, H_2O_2 was generated by the reduction of dissolved oxygen Eq. (1), which reacted with Fe^{2+} which was dissolved from SZVI, (Eq. (3)) to produce $^{\bullet}$OH radicals Eq. (4) that can degrade organic pollutants. Additionally, textile industry effluents can be decontaminated by another type of indirect EO process, with chlorine species generated by graphite electrodes [42]. Therefore, two types of indirect oxidation processes are expected to occur. The first is EO with active chlorine, termed "indirect oxidation" or "Cl^--mediated oxidation" [43], where the anodic oxidation of Cl^- present in the effluent yields active chlorine species (dissolved Cl_2, HClO, and/or OCl^-) and chlorite, chlorine dioxide, chlorate, and perchlorate, which can then oxidize organic pollutants in the bulk [18]. The second is the EF process, in which organics can be destroyed by homogeneous $^{\bullet}$OH formed from the Fenton reaction between Fe^{2+} (dissolved from SZVI) and H_2O_2 electrogenerated from O_2 reduction on a suitable cathode [17]. In both cases, contaminants are competitively destroyed by direct anodic oxidation and reacting with heterogeneous M($^{\bullet}$OH), other ROS and weaker oxidants produced by the oxidation of water and anions in the electrolyte. For real wastewater from the textile industry, this process is very complex, with several reactions that are unlikely to be explained or predicted. However, to a first approximation, it can be assumed that the consumption of $^{\bullet}$OH radicals by organic matter (OM) can be represented by a simple irreversible reaction regarding COD or TOC (fundamental parameters for determining the efficiency of the treatment system and water quality), as shown in Eqs. (14) and (15) [44].

$$OM + HO^{\bullet} \rightarrow Intermediates \quad (14)$$

$$Intermediates + HO^{\bullet} \rightarrow CO_2 + H_2O + inorganic\ acids \quad (15)$$

Pseudo-first-order Eqs. (16) and (17) and pseudo-second-order Eqs. (18) and (19) kinetic models were analyzed for COD and TOC as a function of time, as illustrated in Fig. 3. Table 4 presents the kinetic parameters, degradation rate (r_0), rate constant (k), R^2, R^2_{Adj}, and AIC; it can be seen that the r_0 of the COD is greater than that of mineralization (39% and 50% for the first- and second-order models, respectively). This decrease in mineralization is most likely due to the generation of intermediate reaction products, such as organochlorine compounds, alkyl amines, and other aliphatic compounds that compete with the $^{\bullet}$OH radicals and that have a greater resistance to sequential treatment [44]. In addition, the second-order models exhibit higher degradation rates of COD and mineralization than the first-order models. Similar results have been reported by other authors [45].

To select a reaction order, one must determine which transformation is better fitted by a linear regression. Both models have very high

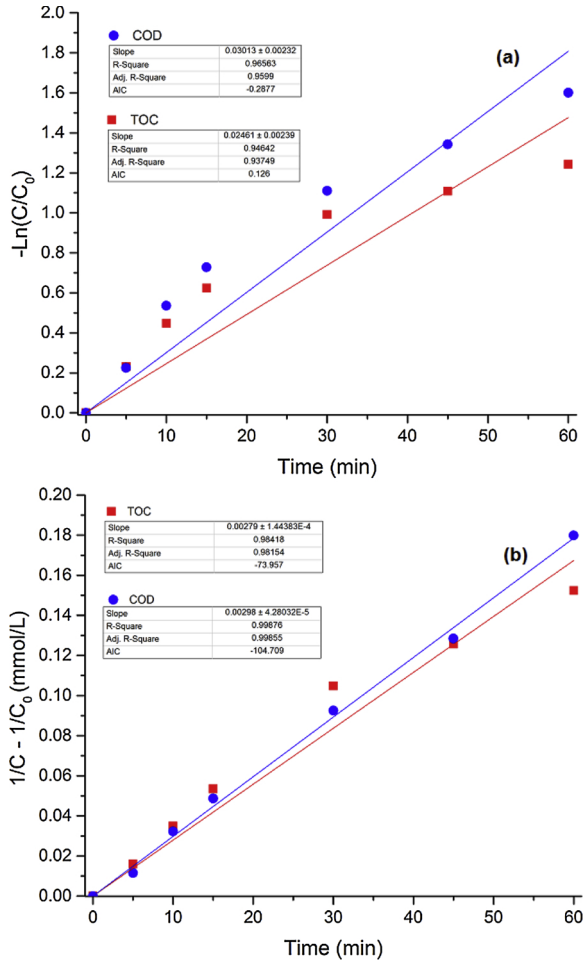

Fig. 3. Kinetic models (a). pseudo First-order and (b) pseudo second-order models for COD and TOC. (pH = 3.5, SZVI = 0.6 g/L, and j = 20 mA/cm^2).

R^2 and R^2_{Adj} values; therefore, the AIC (an objective parameter that quantifies the suitability of a particular model in relation to a set of models [46]) was used to compare the linear regressions of the transformed data for each kinetic model and identify the best alternative. A lower AIC value suggests that the model fits the data better, it is less complex, or a combination of both factors. The AIC was calculated using the statistical software R (https://www.r-project.org/). According to the determined AIC values, the pseudo-second-order kinetic model is the most appropriate both for the COD and TOC.

Pseudo-first-order kinetic model

$$r_0 = -\frac{d(OM)}{dt} = k_1[OM] \quad (16)$$

$$Ln\left(\frac{OM_0}{OM}\right) = k_1 * t \quad (17)$$

Pseudo-second-order kinetic model

$$r_0 = -\frac{d(OM)}{dt} = k_2[OM]^2 \quad (18)$$

$$\frac{1}{OM} - \frac{1}{OM_0} = k_2 * t \quad (19)$$

Other authors, such as Kaur et al. [38] and Parsa et al. [47], have effectively adjusted EO data to pseudo-first-order models most likely because these authors primarily studied surface-mediated processes and the dependence of the degradation rate on the pollutant concentration as well as SZVI-mediated processes, as reported by Donadelli et al. [39] and Ghanbari et al. [45]. None of these previous works provided a comparison with the second-order kinetics, which seem to fit our model better based on the AIC; however, although the second-order kinetics fit our results better, the first-order equations also fit the EO/SZVI experimental data.

To better investigate the contribution of the different possible oxidant species to the degradation, *t*ert-butyl alcohol (*t*-BuOH) and benzoquinone (BQ) were used as specific scavengers for $^{\bullet}$OH radicals and $O_2^{\bullet-}$, respectively, and the results are depicted in Fig. S4 (Supplemental Information). The EO/SZVI process without scavengers achieved a %DTOC of 71%, which decreased to 54.5% and 43.6% when BQ and *t*-BuOH were added, respectively. The decrease in %DTOC in the presence of *t*-BuOH suggests that $^{\bullet}$OH radicals are active species during EO/SZVI treatment; while its decrease in the presence of BQ indicates the existence of the $O_2^{\bullet-}$ species in the degradation process. In addition, the observed degradation rate (r_0) decreased from 0.66 to 0.34 and 0.22 mM/min when BQ and *t*-BuOH were added to the reaction, respectively. These results suggest that both $^{\bullet}$OH and $O_2^{\bullet-}$ species were involved in the EO/SZVI process and were the primary species responsible for the degradation of textile wastewater during the treatment. The stronger trapping effect for *t*-BuOH compared with BQ indicates that $^{\bullet}$OH radicals, which are likely generated by the Fenton process, were the predominant species during the EO/SZVI treatment. These results agree with previous reports, such as that by Saleh and Taufik [48], who found similar results when investigating the Fenton, photo-Fenton, and sono-Fenton processes for the degradation of methylene blue and congo red using BQ and *t*-BuOH scavengers.

Based on the above analysis, a possible mechanism for the degradation in the EO/SZVI process (Fig. S4, Supplemental Information) is proposed. In the EO/SZVI process with electrogenerated H_2O_2 Eq. (1), $^{\bullet}$OH radicals from both anodic and cathodic sources act together to strongly oxidize organic pollutants in wastewater, either by H atom abstraction (producing H_2O) or via $^{\bullet}$OH addition to multiple bonds and intermediate radicals (hydroxylation). The performance of the EO/SZVI process can be attributed to the simultaneous occurrence of more complex reactions, including oxidation–reduction SZVI Eq. (2), the coagulation of iron hydroxides, direct electrochemical oxidation at the graphite anode, indirect electrochemical oxidation by electrogenerated oxidants ($^{\bullet}$OH, H_2O_2, Cl_2, HClO, and/or OCl^-, etc.), and Fenton's reaction Eqs. (2 and 4). EO/SZVI processes seem to be attractive because the mineralization rates of organic pollutants are higher than those for either electrochemical oxidation or the Fenton reaction. This high efficiency is partially due to the continuous generation of H_2O_2 at the cathode and because under acidic conditions, SZVI oxidizes to Fe^{2+} and reacts with H_2O_2 to generate more $^{\bullet}$OH radicals.

3.6. Synergy of effects

To thoroughly evaluate the interaction between the EO process and

Table 4
Kinetic parameters of the EO/SZVI reaction.

Kinetic Model	k'	R^2	R^2_{Adj}	r_o (mM/min)	AIC
1st order (COD) (min^{-1})	0.030 ± 0.0023	0.9656	0.9599	0.66 ± 7.8*10^{-3}	−0.2877
2nd order (COD) (L/mmol-min)	0.003 ± 4.3*10^{-5}	0.9988	0.9986	1.45 ± 1.5*10^{-2}	−73.96
1st order (TOC) (min^{-1})	0.025 ± 0.0023	0.9464	0.9375	0.41 ± 5.8*10^{-2}	0.126
2nd order (TOC) (L/mmol-min)	0.0028 ± 1.44*10^{-4}	0.9842	0.9815	0.73 ± 6.2*10^{-2}	−104.709

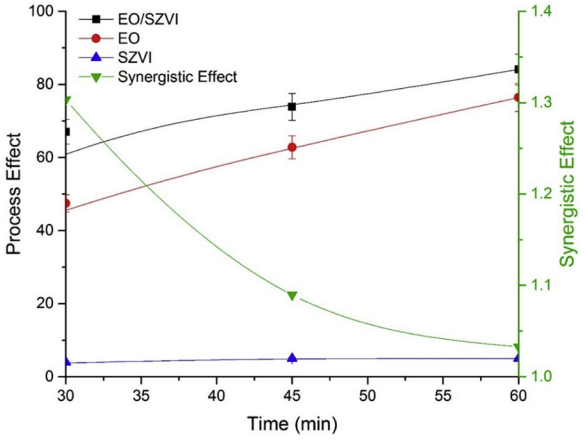

Fig. 4. Synergistic effect during the reaction time in the EO/SZVI (■) process under optimal conditions (pH = 3.5, SZVI = 0.6 g/L, j = 20 mA/cm^2). EO (●) (pH = 3.5, j = 20 mA/cm^2). SZVI (▲) (pH = 3.5, SZVI = 0.6 g/L). The error bars (smaller than the symbol if not visible) indicate the standard deviation.

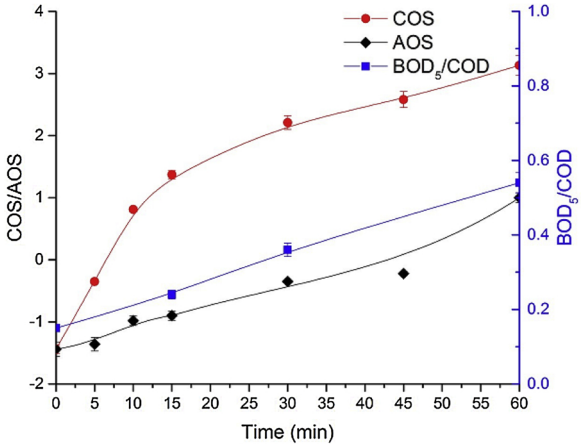

Fig. 5. Average oxidation state (AOS), carbon oxidation state (COS), and BOD_5/COD ratio during 60 min of EO/SZVI treatment under optimal conditions (pH = 3.5, SZVI = 0.6 g/L, and j = 20 mA/cm^2). The error bars (smaller than the symbol if not visible) indicate the standard deviation.

the addition of SZVI, the synergistic effect of the reactions was calculated as follows:

$$Synergystic\ effect = \frac{COD_{EO/SZVI}}{COD_{EO} + COD_{SZVI}}. \quad (20)$$

Here, the effect of the entire process is compared with the sum of the effects of the individual processes. A synergistic effect value exceeding unity suggests an effect due to an interaction between the individual reactions.

Fig. 4 shows the synergistic effect during the reaction time, with the value exceeding unity during the entire period. However, the synergistic effect diminishes with time, most likely due to the decrease in the reaction rate, as shown in Fig. 2(a). This behavior suggests that SZVI primarily contributes to the process by increasing the reaction rate, thereby substantially reducing the OC.

The removal percentage of COD in the EO/SZVI process (Fig. 4) was greater than that for EO and SZVI. The higher degradation efficiency for EO/SZVI in comparison with EO occurs because SZVI oxidizes to Fe^{2+}, which then reacts with H_2O_2 to generate $^{\bullet}OH$ radicals. These radicals are more efficient under acidic conditions, as shown in Eqs. (1–4). Further, the %DCOD can be enhanced by the direct reaction between SZVI and H_2O_2, which generates more $^{\bullet}OH$ radicals [36].

3.7. Analysis of post-process pollutants: toxicity and biodegradability

Additional information regarding the behavior of OM during the process can be obtained by analyzing the average oxidation state (AOS) and carbon oxidation state (COS), which are calculated as follows [49]:

$$COS = 4 - 1.5*(\frac{COD}{TOC_0}), \quad (21)$$

$$AOS = 4 - 1.5*(\frac{COD}{TOC}), \quad (22)$$

where TOC_0 and TOC are the initial TOC and that at the sampling time, respectively, and COD is the COD at the sampling time (all parameters are expressed in units of mg/L). Notice that the COS considers TOC_0, whereas the AOS considers TOC, which is because the CO_2 eliminated from the solution (oxidation state +4) is considered in the COS calculation and only the organic compounds remaining in the solution are considered in the AOS calculation. The AOS is therefore used to identify variations in the sample that could change its biodegradability, and the COS is considered an indicator of the process efficiency [50].

During the EO/SZVI process, both the COS and AOS increased with time, as shown in Fig. 5. The final COS value of approximately 3 suggests that the OM in the post-process sample comprised mainly organic acids, and the increase in the AOS shows enhanced biodegradability, which is also noticeable in the increased biodegradability index (BOD_5/COD). It has been reported that a biodegradability index higher than 0.4 is acceptable for water discharges [6], and because the EO/SZVI process achieved a value of 0.54, it seems logical to conclude that the effluent is sufficiently biodegradable to be discharged.

It has been reported that several organic acids can be formed as reaction intermediates, such as tartaric, formic, oxalic, and fumaric acids, which are formed by the oxidation of azo dyes. Their formation depends on the initial dye concentration, and some intermediates are more stable and toxic than their parent compounds [36]. To further analyze the evolution of organic compounds during the EO/SZVI process, the acids in the samples were characterized by MWD and HPLC during 60 min of the process, as shown in Fig. 6. Ion-exclusion chromatograms showed the presence of some short-linear-chain acids that were formed as intermediaries of the EO/SZVI process. Oxalic [retention time (rt) = 7.2 min], tartaric (rt = 9.6 min), and fumaric (rt = 16.1 min) acids were detected. Notice that the concentration of the acids that were identified corresponds to 70% of the TOC; according to the HPLC analysis, 39 out of 56 ppm of the OM corresponds to the aforementioned acids, and the remainder corresponds to other organic

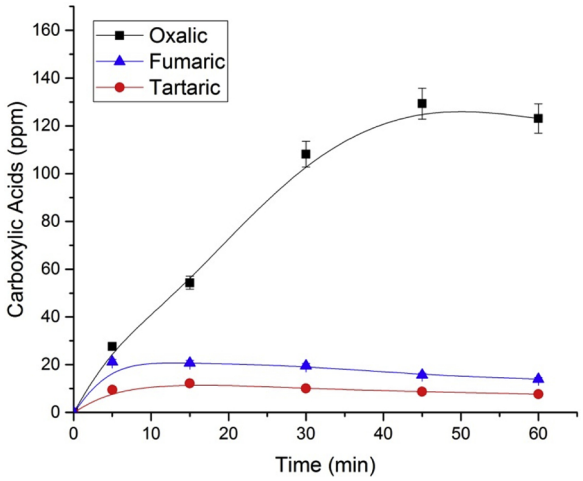

Fig. 6. Evolution of carboxylic acids generated during the degradation of TIWW by EO/SZVI treatment under optimal conditions (pH = 3.5, SZVI = 0.6 g/L, and j = 20 mA/cm^2). The error bars (smaller than the symbol if not visible) indicate the standard deviation.

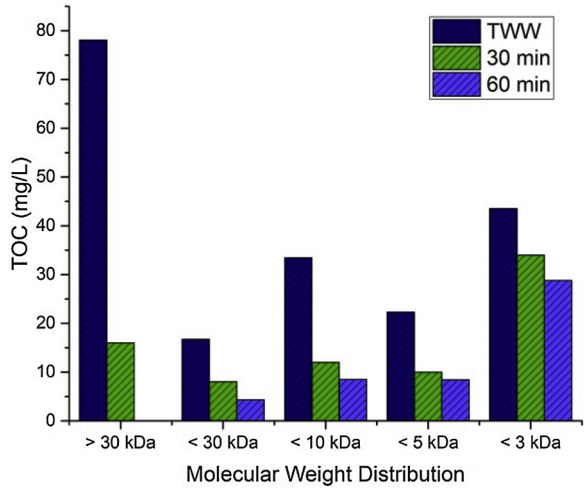

Fig. 7. Molecular weight distribution (MWD) of EO/SZVI treatment under optimal conditions (pH = 3.5, SZVI = 0.6 g/L, and j = 20 mA/cm^2).

compounds such as organochlorinated compounds and aromatics.

The MWD showed that the initial TIWW comprised mainly OM with high MW, as shown in Fig. 7. However, this fraction had degraded completely after 60 min of the EO/SZVI process, yielding a sample that was polluted mostly by compounds of low MW, which are more likely to be biodegraded; this is in agreement with the results presented previously.

3.8. Toxicity of treated samples

In addition to organic acids and possibly toxic intermediaries, it is widely known that the EO process may generate organochlorine compounds in the presence of chlorine, these being of higher toxicity than their predecessors [18]. Fig. 8 illustrates the effect of acute toxicity on *A. salina* in the sample. Notice that the TIWW sample caused a mortality of 100% that remained after runs of both 30 and 60 min even though the biodegradability had increased significantly; this was probably due to the formation of compounds with high toxicity. Therefore, the EF-treated wastewater is still lethal to aquatic life and requires additional treatment to lower its toxicity further before being disposed of in the environment.

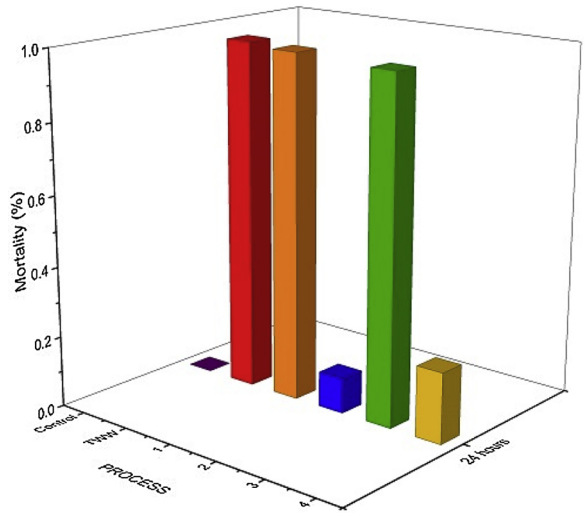

Fig. 8. Mortality of *A. salina* during each step of EO/SZVI treatment under optimal conditions (pH = 3.5, SZVI = 0.6 g/L, and j = 20 mA/cm^2). 1: EO/SZVI (30 min); 2: EO/SZVI (30 min) + AC (4 h); 3: EO/SZVI (60 min); 4: EO/SZVI (60 min) + AC (4 h).

Because of the high toxicity of the post-process sample, experimental runs were performed for EO/SZVI combined with AC. Samples subjected to 30 or 60 min of EO/SZVI treatment were stirred with 10 g/L AC for 4 h; subsequently, the AC was isolated, and the toxicity was measured. The incorporation of AC greatly reduced the toxicity of the samples, yielding mortality rates of 10% and 20% in the samples treated for 30 and 60 min, respectively, which agrees with previous work [25].

3.9. Reuse potential of the SZVI catalyst during EO/SZVI treatment

Stability is significant for applications when considering the use of a SZVI catalyst in the EO/SZVI process. Therefore, to evaluate the reuse potential, several test runs under optimum conditions (pH = 3.5, SZVI = 0.6 g/L, and j = 20 mA / cm^2 for 30 min) were performed while reusing the same SZVI load for each consecutive run until a drop in the process efficiency (%DCOD or %DTOC) was observed. After each cycle, the remaining SZVI particles were vacuum filtered, washed with 5 mL of DI water three times, and vacuum dried for use in the next cycle. The results show that the degradation of COD and TOC remained similar over six runs, with values of 84%, 84%, 82%, 82%, 80%, and 80% for %DCOD and 71%, 70%, 69%, 69%, 68%, and 67% for %DTOC; the process efficiency then decreased significantly, indicating that the EO/SZVI process remains stable over 6 runs with reused SZVI.

4. Conclusions

The experimental results in this work show the effectiveness of the EO/SZVI process for degrading persistent pollutants with low biodegradability in a TIWW effluent. The optimal operating conditions for decreasing the cost while maintaining sufficient degradation for discharge were an SZVI concentration of 0.6 g/L, pH of 3.5, and a current density of 20 mA/cm^2, which were found using a BBD and response-surface methodology. These conditions led to color, COD, and TOC reductions of 100%, 67%, and 59%, respectively, in 30 min of reaction.

The SZVI was found to accelerate the organic-matter degradation in the EO process, leading to a reduction in the reaction time required to achieve an effluent ready for discharge. Also, degradation in the EO/SZVI process seems to adjust to a pseudo-second order kinetic model. Experimental runs with scavengers (BQ and *t*-Bu − OH) suggest that degradation in the EO/SZVI occurs mainly because of the generation of $^{\bullet}$OH radicals, that can be either electrogenerated or by the reaction of electrogenerated H_2O_2 and Fe^{2+} released from the surface of SZVI.

Additionally, the biodegradability index increased from 0.15 to 0.4, and the AOS increased from −1.44 to 1, suggesting an increase in the biodegradability of the process. Meanwhile, the acute toxicity to *A. salina* decreased from 100% to 10% with an additional AC adsorption step, indicating that the final effluent was nontoxic and sufficiently biodegradable to be discharged.

The HPLC analysis showed that the final effluent comprised mainly oxalic, fumaric, and tartaric acids, which corresponded to 74% of the organic carbon. This was also supported by a COS value of around 3, suggesting that the effluent comprised mainly organic acids. Furthermore, the MWD showed the absence of pollutants with an MW higher than 30 kDa in the final effluent, which comprised mainly pollutants with an MW lower than 3 kDa (58% of the organic carbon).

Experimental runs showed that the SZVI can be reused around 6 times without compromising degradation. This leads to a process cost of 3.4 USD/m^3, which is lower than that of some processes reported in previous EO and EF works [18,25]. Moreover, considering the rapid increase in biodegradability, optimizing the process with the objective of biodegradability could be considered for coupling this process with biological processes to attain an even lower OC.

Declaration of Competing Interest

There are no known conflicts of interest.

Acknowledgments

The authors thank the Dirección de Investigación de la Universidad EAFIT, Medellín–Colombia for supporting this research financially and the staff of the Laboratorio de Ingeniería de Procesos for their assistance.

Appendix A. Supplementary data

Supplementary material related to this article can be found, in the online version, at doi:https://doi.org/10.1016/j.jwpe.2019.100924.

References

[1] S.O. Ganiyu, M. Zhou, C.A. Martínez-Huitle, Heterogeneous electro-Fenton and photoelectro-Fenton processes: a critical review of fundamental principles and application for water/wastewater treatment, Appl. Catal. B Environ. 235 (2018) 103–129, https://doi.org/10.1016/j.apcatb.2018.04.044.

[2] E. Brillas, A review on the degradation of organic pollutants in waters by UV Photoelectro Fenton and solar photoelectro-fenton, J. Braz. Chem. Soc. 25 (2014) 393–417.

[3] A.U. Souza, L.G.M. Silva, F.C. Moreira, S.M.A.G.U. Souza, R.A.R. Boaventura, V.J.P. Vilar, Chemical and electrochemical advanced oxidation processes as a polishing step for textile wastewater treatment : a study regarding the discharge into the environment and the reuse in the textile industry, J. Clean. Prod. 198 (2018) 430–442, https://doi.org/10.1016/j.jclepro.2018.07.001.

[4] E. GilPavas, I. Dobrosz-gómez, M.Á. Gómez-garcía, Optimization of sequential chemical coagulation - electro-oxidation process for the treatment of an industrial textile wastewater, J. Water Process Eng. 22 (2018) 73–79, https://doi.org/10.1016/j.jwpe.2018.01.005.

[5] C.R. Holkar, A.J. Jadhav, D.V. Pinjari, N.M. Mahamuni, A.B. Pandit, A critical review on textile wastewater treatments: possible approaches, J. Environ. Manage. 182 (2016) 351–366, https://doi.org/10.1016/j.jenvman.2016.07.090.

[6] F. Ghanbari, M. Moradi, A comparative study of electrocoagulation, electrochemical Fenton, electro-Fenton and peroxi-coagulation for decolorization of real textile wastewater: electrical energy consumption and biodegradability improvement, J. Environ. Chem. Eng. 3 (2015) 499–506, https://doi.org/10.1016/j.jece.2014.12.018.

[7] B. Bethi, S.H. Sonawane, B.A. Bhanvase, S.P. Gumfekar, Nanomaterials-based advanced oxidation processes for wastewater treatment: a review, Chem. Eng. Process. Process Intensif. 109 (2016) 178–189, https://doi.org/10.1016/j.cep.2016.08.016.

[8] M. Gągol, A. Przyjazny, G. Boczkaj, Wastewater treatment by means of advanced oxidation processes based on cavitation – a review, Chem. Eng. J. 338 (2018) 599–627, https://doi.org/10.1016/j.cej.2018.01.049.

[9] F.C. Moreira, R.A.R. Boaventura, E. Brillas, V.J.P. Vilar, Electrochemical advanced oxidation processes: a review on their application to synthetic and real wastewaters, Appl. Catal. B Environ. 202 (2017) 217–261, https://doi.org/10.1016/j.apcatb.2016.08.037.

[10] M. Kahoush, Bio-Fenton and Bio-electro-Fenton as sustainable methods for degrading organic pollutants in wastewater, Process Biochem. 64 (2018) 237–247, https://doi.org/10.1016/j.procbio.2017.10.003.

[11] E. GilPavas, I. Dobrosz-Gómez, M.Á. Gómez-García, Optimization of solar-driven photo-electro-Fenton process for the treatment of textile industrial wastewater, J. Water Process Eng. 24 (2018) 49–55, https://doi.org/10.1016/j.jwpe.2018.05.007.

[12] K. Jüttner, U. Galla, H. Schmieder, Electrochemical approaches to environmental problems in the process industry, Electrochim. Acta 45 (2000) 2575–2594, https://doi.org/10.1016/S0013-4686(00)00339-X.

[13] V. Poza-Nogueiras, E. Rosales, M. Pazos, M. Sanromán, Current advances and trends in electro-Fenton process using heterogeneous catalysts – a review, Chemosphere 201 (2018) 399–416, https://doi.org/10.1016/j.chemosphere.2018.03.002.

[14] P. Kaur, J.P. Kushwaha, V.K. Sangal, Chemosphere Transformation products and degradation pathway of textile industry wastewater pollutants in Electro-Fenton process, Chemosphere 207 (2018) 690–698, https://doi.org/10.1016/j.chemosphere.2018.05.114.

[15] P. Kaur, V. Sangal, J. Kushwaha, Parametric study of Electro-Fenton treatment for real textile wastewater, disposal study and its cost analysis, Int. J. Environ. Sci. Technol. (Tehran) 16 (2018) 1735–2630, https://doi.org/10.1007/s13762-018-1696-9.

[16] S. Ganiyu, T. Le, M. Bechelany, G. Esposito, E. Van Hullebusch, M. Oturan, M. Cretin, Hierarchical CoFe-Layered double hydroxide modified carbon-felt cathode for heterogeneous electro-fenton process, J. Mater. Chem. A Mater. Energy Sustain. (2017).

[17] E. Brillas, I. Sirés, M. Oturan, Electro-fenton process and related electrochemical technologies based on Fenton's reaction chemistry, Chem. Rev. 109 (2009) 6570–6631.

[18] E. Brillas, Ca. Martinez-Huitle, Decontamination of wastewaters containing synthetic organic dyes by electrochemical methods, An updated review, Appl. Catal. B Environ. 166-167 (2015) 603–643, https://doi.org/10.1016/j.apcatb.2014.11.016.

[19] C.M. Sánchez-Sánchez, E. Expósito, J. Casado, V. Montiel, Goethite as a more effective iron dosage source for mineralization of organic pollutants by electro-Fenton process, Electrochem. Commun. 9 (2007) 19–24, https://doi.org/10.1016/j.elecom.2006.08.023.

[20] E. Expósito, C.M. Sánchez-Sánchez, V. Montiel, Mineral Iron oxides as Iron source in Electro-Fenton and photoelectro-fenton mineralization processes, J. Electrochem. Soc. 154 (2007) E116, https://doi.org/10.1149/1.2744134.

[21] Y. Segura, F. Martínez, J.A. Melero, J.L.G. Fierro, Zero valent iron (ZVI) mediated Fenton degradation of industrial wastewater : treatment performance and characterization of final composites, Chem. Eng. J. 269 (2015) 298–305, https://doi.org/10.1016/j.cej.2015.01.102.

[22] A. Kumar, S. Jena, B.C. Acharya, B.K. Mishra, Removal of azo dye in innovative constructed wetlands : influence of iron scrap and sulfate reducing bacterial enrichment, Ecol. Eng. 49 (2012) 53–58, https://doi.org/10.1016/j.ecoleng.2012.08.032.

[23] P. Lai, H. Zhao, C. Wang, J. Ni, Advanced treatment of coking wastewater by coagulation and zero-valent iron processes, J. Hazard. Mater. 147 (2007) 232–239, https://doi.org/10.1016/j.jhazmat.2006.12.075.

[24] B. Kakavandi, A. Takdastan, S. Pourfadakari, M. Ahmadmoazzam, S. Jorfi, Heterogeneous catalytic degradation of organic compounds using nanoscale zero-valent iron supported on kaolinite: mechanism, kinetic and feasibility studies, J. Taiwan Inst. Chem. Eng. 96 (2019) 329–340, https://doi.org/10.1016/j.jtice.2018.11.027.

[25] E. GilPavas, I. Dobrosz-Gómez, M.-Á. Gómez-García, Optimization and toxicity assessment of a combined electrocoagulation, H_2O_2/Fe^{2+}/UV and activated carbon adsorption for textile wastewater treatment, Sci. Total Environ. 651 (2019) 551–560, https://doi.org/10.1016/j.scitotenv.2018.09.125.

[26] P.O. Bankole, A.A. Adekunle, O.F. Obidi, O.D. Olukanni, S.P. Govindwar, Degradation of indigo dye by a newly isolated yeast, Diutina rugosa from dye wastewater polluted soil, J. Environ. Chem. Eng. 5 (2017) 4639–4648, https://doi.org/10.1016/j.jece.2017.08.050.

[27] R.E. Palma-goyes, J. Silva-agredo, I. González, R.A. Torres-palma, Comparative degradation of indigo carmine by electrochemical oxidation and advanced oxidation processes, Electrochim. Acta 140 (2014) 427–433, https://doi.org/10.1016/j.electacta.2014.06.096.

[28] K. Hendaoui, F. Ayari, I. Ben, R. Ben, F. Darragi, Real indigo dyeing effluent decontamination using continuous electrocoagulation cell : study and optimization using Response Surface Methodology, Process Saf. Environ. Prot. 116 (2018) 578–589, https://doi.org/10.1016/j.psep.2018.03.007.

[29] O. Tünay, ̧Merve Simseker, I. Kabdaslı, T. Ölmez-Hancı, Abatements of reduced sulphur compounds, colour, and organic matter from indigo dyeing effluents by electrocoagulation, Environ. Technol. (2014) 1577–1588, https://doi.org/10.1080/09593330.2013.873824.

[30] M. Kallel, C. Belaid, R. Boussahel, M. Ksibi, A. Montiel, B. Elleuch, Olive mill wastewater degradation by Fenton oxidation with zero-valent iron and hydrogen peroxide, J. Hazard. Mater. 163 (2009) 550–554, https://doi.org/10.1016/j.jhazmat.2008.07.006.

[31] Standard Methods for the Examination of Water and Wastewater, 22nd ed., American Public Health Association (APHA), American Water Works Association (AWWA), Water Environmental Federation (WEF), Washington, D.C, 2012.

[32] L. Manfra, S. Canepa, V. Piazza, M. Faimali, Lethal and sublethal endpoints observed for Artemia exposed to two reference toxicants and an ecotoxicological concern organic compound, Ecotoxicol. Environ. Saf. 123 (2016) 60–64, https://doi.org/10.1016/j.ecoenv.2015.08.017.

[33] S. Mortazavian, H. An, D. Chun, J. Moon, Activated carbon impregnated by zero-valent iron nanoparticles (AC/nZVI) optimized for simultaneous adsorption and reduction of aqueous hexavalent chromium : material characterizations and kinetic studies, Chem. Eng. J. 353 (2018) 781–795, https://doi.org/10.1016/j.cej.2018.07.170.

[34] G.E. Box, J.S. Hunter, W.G. Hunter, Statistics for Experimenters: Design, Innovation, and Discovery, 2nd ed., Wiley-Interscience, New York, 2005.

[35] B.M. da Costa Filho, V.M. da Silva, J. de O. Silva, A.E. da Hora Machado, A.G. Trovó, Coupling coagulation, flocculation and decantation with photo-Fenton process for treatment of industrial wastewater containing fipronil: biodegradability and toxicity assessment, J. Environ. Manage. 174 (2016) 71–78, https://doi.org/10.1016/j.jenvman.2016.03.019.

[36] S. Garcia-segura, A. El-ghenymy, F. Centellas, R.M. Rodríguez, C. Arias, J.A. Garrido, P.L. Cabot, E. Brillas, Comparative degradation of the diazo dye Direct Yellow 4 by electro-Fenton, photoelectro-Fenton and photo-assisted electro-Fenton, J. Electroanal. Chem. Lausanne (Lausanne) 681 (2012) 36–43, https://doi.org/10.1016/j.jelechem.2012.06.002.

[37] X. Li, L. Ai, J. Jiang, Nanoscale zerovalent iron decorated on graphene nanosheets for Cr (VI) removal from aqueous solution : surface corrosion retard induced the enhanced performance, Chem. Eng. J. 288 (2016) 789–797, https://doi.org/10.1016/j.cej.2015.12.022.

[38] P. Kaur, J.P. Kushwaha, V.K. Sangal, Electrocatalytic oxidative treatment of real textile wastewater in continuous reactor: degradation pathway and disposability study, J. Hazard. Mater. 346 (2018) 242–252, https://doi.org/10.1016/j.jhazmat.2017.12.044.

[39] J.A. Donadelli, L. Carlos, A. Arques, F.S. García, Environmental Kinetic and mechanistic analysis of azo dyes decolorization by ZVI-assisted Fenton systems: pH-dependent shift in the contributions of reductive and oxidative transformation pathways, Appl. Catal. B Environ. 231 (2018) 51–61, https://doi.org/10.1016/j.

apcatb.2018.02.057.
[40] X. Zhu, J. Ni, Electrochimica Acta the improvement of boron-doped diamond anode system in electrochemical degradation of p -nitrophenol by zero-valent iron, Electrochim. Acta 56 (2011) 10371–10377, https://doi.org/10.1016/j.electacta.2011.05.062.
[41] H.M. Pinheiro, E. Touraud, O. Thomas, Aromatic amines from azo dye reduction : status review with emphasis on direct UV spectrophotometric detection in textile industry wastewaters, Dye. Pigment. 61 (2004) 121–139, https://doi.org/10.1016/j.dyepig.2003.10.009.
[42] P. Kariyajjanavar, N. Jogttappa, Y. Arthoba, Studies on degradation of reactive textile dyes solution by electrochemical method, J. Hazard. Mater. 190 (2011) 952–961, https://doi.org/10.1016/j.jhazmat.2011.04.032.
[43] A.M. Sales Solano, J. Costa de Araújo, C.K. Vieira de Melo, J.M. Peralta-hernandez, D. Ribeiro da Silva, C.A. Martínez-huitle, Applied Catalysis B : environmental Decontamination of real textile industrial effluent by strong oxidant species electrogenerated on diamond electrode : viability and disadvantages of this electrochemical technology, Applied Catal. B, Environ. 130–131 (2013) 112–120, https://doi.org/10.1016/j.apcatb.2012.10.023.
[44] I. Oller, S. Malato, J.A. Sánchez-Pérez, W. Gernjak, M.I. Maldonado, L.A. Pérez-Estrada, C. Pulgarín, A combined solar photocatalytic-biological field system for the mineralization of an industrial pollutant at pilot scale, Catal. Today 122 (2007) 150–159, https://doi.org/10.1016/j.cattod.2007.01.041.
[45] F. Ghanbari, M. Moradi, M. Manshouri, Textile wastewater decolorization by zero valent iron activated peroxymonosulfate: compared with zero valent copper, J. Environ. Chem. Eng. 2 (2014) 1846–1851, https://doi.org/10.1016/j.jece.2014.08.003.
[46] M. Snipes, D.C. Taylor, Model selection and Akaike Information Criteria: an example from wine ratings and prices, Wine Econ. Policy. 3 (2014) 3–9, https://doi.org/10.1016/j.wep.2014.03.001.
[47] J.B. Parsa, M. Rezaei, A.R. Soleymani, Electrochemical oxidation of an azo dye in aqueous media investigation of operational parameters and kinetics, J. Hazard. Mater. 168 (2009) 997–1003, https://doi.org/10.1016/j.jhazmat.2009.02.134.
[48] R. Saleh, A. Taufik, Degradation of methylene blue and congo-red dyes using Fenton, photo-Fenton, sono-Fenton, and sonophoto-Fenton methods in the presence of iron(II,III) oxide/zinc oxide/graphene (Fe_3O_4/ZnO/graphene) composites, Sep. Purif. Technol. 210 (2019) 563–573, https://doi.org/10.1016/j.seppur.2018.08.030.
[49] D.R. Manenti, A.N. Módenes, Pa. Soares, F.R. Espinoza-Quiñones, Ra R. Boaventura, R. Bergamasco, V.J.P. Vilar, Assessment of a multistage system based on electrocoagulation, solar photo-Fenton and biological oxidation processes for real textile wastewater treatment, Chem. Eng. J. 252 (2014) 120–130, https://doi.org/10.1016/j.cej.2014.04.096.
[50] C.A. Masiello, M.E. Gallagher, J.T. Randerson, R.M. Deco, O.A. Chadwick, Evaluating two experimental approaches for measuring ecosystem carbon oxidation state and oxidative ratio, J. Geophys. Res. (2008) 0–9, https://doi.org/10.1029/2007JG000534.